Available online at www.sciencedirect.com

ScienceDirect

Procedia Manufacturing 38 (2019) 1252–1259

Procedia MANUFACTURING

www.elsevier.com/locate/procedia

29th International Conference on Flexible Automation and Intelligent Manufacturing (FAIM2019), June 24-28, 2019, Limerick, Ireland.

Fracture envelope estimation of a structural adhesive by dedicated fracture tests

F.A.A. Nunes[a], R.D.S.G. Campilho[a,b,*], M.G. Cardoso[a], F.J.G. Silva[a]

[a]*ISEP-School of Engineering, Rua Dr. António Bernardino de Almeida 431, 4200-072 Porto, Portugal*
[b]*INEGI, Campus da FEUP, Rua Dr. Roberto Frias 400, 4200-465 Porto, Portugal*

Abstract

Cohesive zone modelling (CZM) is widespread for the strength analysis of bonded joints. The fracture toughness (G_C) is required to use CZM. A scarcely studied mixed-mode test is the Asymmetric Tapered Double-Cantilever Beam (ATDCB), which merges a Tapered Double-Cantilever Beam (TDCB) adherend with a Double-Cantilever Beam (DCB) adherend. This work addresses the ATDCB test to estimate the fracture envelope of a structural adhesive. TDCB and End-Notched Flexure (ENF) tests were also performed to acquire the tensile (G_{IC}) and shear fracture toughness (G_{IIC}), respectively. Numerically, mixed-mode CZM laws were constructed based on the obtained data, and the results were compared with experiments, to validate the CZM laws and the mixed mode propagation criterion. As a result, the best damage propagation criterion for mixed mode was estimated and validated.

Keywords: Adhesive joints; Structural adhesive; Fracture toughness; Cohesive zone modelling; Fracture envelope.

1. Introduction

Continuum mechanics-based techniques can be applied for the strength prediction of bonded-joints. In this case, the stress distributions are initially estimated by analytical or numerical methods [1]. The maximum load (P_m) is then

* Corresponding author. Tel.: +351-939526892; fax: +351-228321159.
E-mail address: raulcampilho@gmail.com

10.1016/j.promfg.2020.01.217

predicted by comparing peak stresses or strains with the material admissible values. The CZM technique is the most widespread for the strength analysis of bonded joints. In the local approach, the CZM laws are used to connect superimposed nodes of elements of different materials or different composites layers [2]. By the continuous approach, the CZM laws are applied directly between two non-contact materials [3]. The main disadvantage of the continuum approach is that the CZM laws become dependent on the adherends thickness (h) and adhesive thickness (t_A), because they affect the size of the fracture process zone (FPZ) and plasticity in front of the crack tip.

G_C, which represents the crack propagation resistance, is one of the properties required to use CZM. Varying pure-mode loading modes may occur: opening (mode I), shear (mode II) and tearing (mode III). In mode I tests, the joint is under opening loads and the crack propagates perpendicularly to the plane of loading. The DCB test uses adherends with constant h, and it is the most used test in mode I. The TDCB test is another option, and it consists of using tapered adherends, i.e., h increases with the crack length (a). A few tests are available for mode II, such as the ENF and End-Loaded Split (ELS) tests. The ENF configuration promotes a dominant mode II solicitation by loading the sample in three-point bending. The main difference in the ELS test, it is that the sample is clamped at one edge and loaded transversely at the other edge. Disregarding the test, usually shear cracks propagate in a complex way, sometimes accompanied by a micro fracture mechanism [1]. Different tests are available to load adhesive joints in mixed-mode, which consists of a combination between mode I and mode II [4]. The mixed-mode behavior of bonded joints is highly relevant, since adhesive joints in practical applications are typical loaded under these conditions. Some of the most relevant mixed-mode tests are the Mixed-Mode Bending (MMB), the Single-Leg Bending (SLB) and he Fixed-Ratio Mixed-Mode (FRMM) tests. On the other hand, a scarcely studied test for mixed-mode is the ATDCB test [5, 6]. This test merges a tapered TDCB adherend with a straight DCB adherend. The specimen is loaded perpendicularly to the adhesive layer but, due to using adherends with varying stiffness, a mixed-mode loading is created in the adhesive.

This work addresses the mixed-mode ATDCB fracture test to estimate the fracture envelope of a structural adhesive. TDCB and ENF tests were also performed to acquire G_{IC} and G_{IIC}, respectively. Numerically, mixed-mode CZM laws were constructed based on the obtained data, and the respective numerical results were compared with the experimental ones, to achieve validation of the CZM laws and the mixed mode propagation criterion of the adhesive.

2. Experimental work

2.1. Materials

The mechanical properties of the adherends were characterized by Campilho et al. [7], according to the ASTM-E8M-04 standard. For the adherends, a low alloy carbon steel was used (C45E steel). Table 1 presents the tensile and shear mechanical properties of the adhesive tested in this work, which is the ductile epoxy Araldite® 2015. Campilho et al. [8, 9] characterized this adhesive by measuring its mechanical and toughness properties. Bulk samples with dogbone shape were tested to determine the Young's modulus (E), tensile yield stress (σ_y), tensile strength (σ_f) and tensile failure strain (ε_f). The samples and tests were done according to the French Standard NF T 76-142, and six samples were fabricated. Campilho et al. [8] used Thick Adherend Shear Tests (TAST) to characterize the shear behaviour of this adhesive. To estimate G_{IC}, DCB tests were performed, and for G_{IIC}, the ENF test was used. The samples were fabricated as depicted by Leitão et al. [10], and room temperature curing was carried out for one week.

Table 1. Mechanical and fracture properties of the adhesive Araldite® 2015 [8, 9].

Property	**2015**		
Young's modulus, E [GPa]	1.85±0.21	Shear yield stress, τ_y [MPa]	14.6±1.3
Poisson's ratio, ν	0.33 [a]	Shear strength, τ_f [MPa]	17.9±1.8
Tensile yield stress, σ_y [MPa]	12.63±0.61	Shear failure strain, γ_f [%]	43.9±3.4
Tensile strength, σ_f [MPa]	21.63±1.61	Toughness in tension, G_{IC} [N/mm]	0.43±0.02
Tensile failure strain, ε_f [%]	4.77±0.15	Toughness in shear, G_{IIC} [N/mm]	4.70±0.34
Shear modulus, G [GPa]	0.70 [b]		

[a] manufacturer's data

[b] estimated from the Hooke's law using E and ν

2.2. Experimental details

Fig. 1 presents the geometry for the different tests (TDCB, ENF, ATDCB). The joint parameters are defined as: length L=241.3 mm (for the TDCB and ATDCB samples) and half-span between cylinders L=100 mm (for the ENF samples), width b=25.4 mm, h=12.7 mm, t_A=1 mm and initial crack length (a_0), which will be described further.

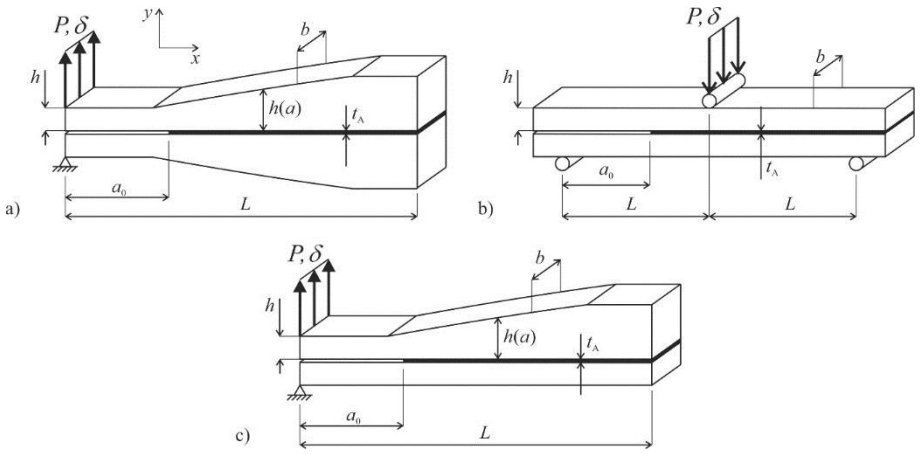

Fig. 1. TDCB (a), ENF (b) and ATDCB specimens (c).

The ISO 25217 standard imposes a specific relation between h and a for the curved adherends of the TDCB and ATDCB adherends, such that the geometric factor m in the next expression is kept constant:

$$m = \frac{3a^2}{h^3} + \frac{1}{h} \tag{1}$$

The main advantage of this relation in the TDCB test is that it enables the compliance (C) to vary linearly with a. This linear function will make the term dC/da constant and, as a result, G_{IC} can be estimated without knowledge of the a values during the test. For the specimens' fabrication, the bonding surfaces were dry blasted in a Cidblast® RT 6S grinding machine, and then cleaned with acetone. To achieve the design value of t_A, steel spacers were placed between the adherends at both edges of the adhesive layer. In order to have an optimum adhesion performance and prevent any misalignment during the cure, the samples were assembled in a steel jig. As recommended by adhesives manufacturer's, the full curing process lasted a week. After, the spacers and the remaining of adhesive were removed. In order to measure the crack growth, a printed metric scale was glued to the side of the samples. A Shimadzu AG-X 100 testing machine with a load cell of 100 kN was used to perform the tests. This equipment provided the load-displacement (P-δ) curve, and crack propagation was recorded using a Canon® EOS 700 D camera.

2.3. G_C estimation

In this work, G_{IC} was estimated by the TDCB test using the Corrected Beam Theory (CBT), and G_{IIC} was assessed by the ENF test considering the Compliance-Based Beam Method (CBBM). Due to the wide application of these methods, these are not described, although their formulation can be found in previous works [10, 11]. The fracture energy (G) estimation method for the ATDCB test considered in this work, further divided into tensile (G_I) and shear components (G_{II}), combines features from both DCB and TDCB tests and it was proposed by Park and Dillard [5]. By this method, the G formulation is based on the Euler Bernoulli beam theory, and it consists of dividing the ATDCB specimen into the equivalent systems depicted in Fig. 2. Since the compliance (C) of the DCB and TDCB tests is already known, the two setups of Fig. 2 enable finding G for the ATDCB test. With this procedure, initially C for the setup of Fig. 2 (b) is found. After, it is considered that this and the setup of Fig. 2 (a) have equal C. From this, it is acceptable to consider that C for the ATDCB test is half that of the setup depicted in Fig. 2 (a).

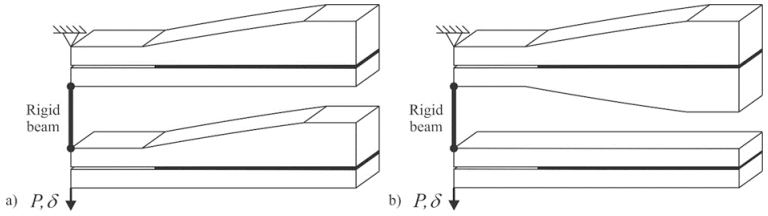

Fig. 2. Equivalent setups to the ATDCB specimen.

C is initially expressed for the system of Fig. 2 (b):

$$C_{\text{total}} = C_{\text{DCB}} + C_{\text{TDCB}}, \tag{2}$$

where C_{DCB} and C_{TDCB} are C for DCB and TDCB tests, respectively. Then, G for the ATDCB test is given by [12]:

$$G = \frac{1}{2}\left(G_{\text{DCB}} + G_{\text{TDCB}}\right) = \frac{1}{2}\left[\frac{P^2}{2b}\frac{d\left(C_{\text{DCB}}\right)}{da} + \frac{P^2}{2b}\frac{d(C_{\text{TDCB}})}{da}\right]. \tag{3}$$

On the other hand, G for the DCB and TDCB tests can be found in reference [13]:

$$G_{\text{DCB}} = \frac{4P^2\left(3a^2 + h^2\right)}{Eb^2h^3} \text{ and } G_{\text{TDCB}} = \frac{4P^2}{Eb^2}m, \tag{4}$$

where m is the aforementioned geometry factor which defines the tapered part of the TDCB adherend. The next system of equations is solved to achieve mode partitioning for the ATDCB test:

$$\begin{cases} \theta = \tan^{-1}\sqrt{\left(\dfrac{G_{\text{II}}}{G_{\text{I}}}\right)} = 24^\circ \\ G = G_{\text{I}} + G_{\text{II}} \end{cases}, \quad \text{with} \quad \begin{cases} G_{\text{I}} = \dfrac{G}{1+\tan^2 24^\circ}. \\ G_{\text{II}} = G - G_{\text{I}} \end{cases} \tag{5}$$

3. Numerical work

3.1. Simulation details

A two-dimensional (2D) analysis in Abaqus® was used in order to reproduce the experimentally obtained behaviour. Plane-strain four-node quadrilateral solid finite elements (CPE4 from Abaqus®) were used to model the adherends, and four-node cohesive elements (COH2D4 from Abaqus®) to model the adhesive. Diverse mesh sizes were used within the models to optimize the simulation, thus guaranteeing accuracy in the stress estimation at the regions of higher gradients. In the adhesive layer and in the adherends close to it, a higher refinement was used, and the elements had edge dimensions of 0.5 mm. The dimensions of adhesive elements were of 0.5×1.0 mm^2, and only one element along its thickness was considered. The boundary conditions consisted of: (1) fixing the lower left node of DCB adherend, (2) restraining the horizontal movement of the upper left node of TDCB adherend and (3) pulling up the same node to induce the experimental loading. All samples were simulated separately by applying the experimentally measured a_0 and considering a CZM law with triangular. These laws were built using G_{IC} and G_{IIC} estimated by TDCB and ENF tests, for similar geometrical and material parameters. Table 1 shows the tensile strength (σ_{f}) and shear strength (τ_{f}) of the adhesive. These parameters were considered, by approximation, equal to the tensile cohesive strength (t_{n}^0) and shear cohesive strength (t_{s}^0), respectively. Section 3.2 describes the α parameter of the energetic crack propagation criterion to be used in the triangular CZM, which is the best match for the adhesive (estimated in Section 4.3). Validation of the CZM laws and parameter α is accomplished by comparing the obtaining the numerical results with experiments.

3.2. Triangular CZM formulation

Relationships among stresses and relative displacements linking similar nodes of cohesive elements are the fundament of the CZM. Additionally, those relations make possible to capture the material's behaviour up to failure [14]. This study relies on triangular pure and mixed-mode laws to model the adhesive layer. Under pure-mode loading, damage initiation occurs when t_n^0 or t_s^0 is attained, i.e., the material's elastic behaviour is cancelled and degradation starts [15]. Furthermore, the crack propagates up to the adjacent pair of nodes when the values of current tensile or shear cohesive stresses (t_n or t_s, respectively) become null. Under mixed-mode loading, stress and/or energetic criteria are often used to combine the pure-mode laws, and damage begins when the mixed mode cohesive strength (t_m^0) is reached [16]. This study focused on the quadratic nominal stress criterion and a power law criterion for the damage initiation and growth, respectively. The Power law criterion is particularly relevant in this work, and it takes the form:

$$\left(\frac{G_I}{G_{IC}}\right)^{\alpha}+\left(\frac{G_{II}}{G_{IIC}}\right)^{\beta}=1, \tag{6}$$

where α and β are constants. In this work, $\alpha=\beta$ was considered. This full model is described in reference [17].

4. Results

4.1. Pure-mode G_{IC} and G_{IIC} estimation

TDCB and ENF tests were considered to obtain G_{IC} and G_{IIC}, respectively. The elastic stiffness and evolution of P in the P-δ curves behaved identically for all tests. The crack growth behaviour was very progressive, without unstable growth regions. The R-curves (plots of G_I or G_{II} vs. a) obtained by the P-δ curves' analysis showed smooth crack growth at approximately constant G_I and G_{II}. The respective average values corresponded to G_{IC} and G_{IIC}, respectively, of each test [18]. This smooth crack growth does not always occur, and oscillations can appear due to inevitable experimental defects such as non-homogeneous adhesive mixing, lack of adhesion, various defects and crack stoppage during the test [19]. The usable crack propagation region is shorter for the ENF than the TDCB test, because the results loose validity when approaching the loading cylinder, which induce compression stresses to the crack tip. As a result, the measured G_{IIC} is no longer valid. The following values were obtained: G_{IC}=0.697±0.0249 N/mm and G_{IIC}=2.798±0.0957 N/mm. It is observed that, for both TDCB and ENF tests, the dispersion of results is low, which can be attested by the reduced percentile standard deviation: 3.6% for G_{IC} and 3.4% for G_{IIC}.

4.2. Mixed-mode G_I and G_{II} estimation

Fig. 3 (a) presents the full batch of ATDCB P-δ curves of the Araldite® 2015. The initial stiffness scatter of the curves was low, and this occurs mainly because of a_0 discrepancies between specimens [10, 11].

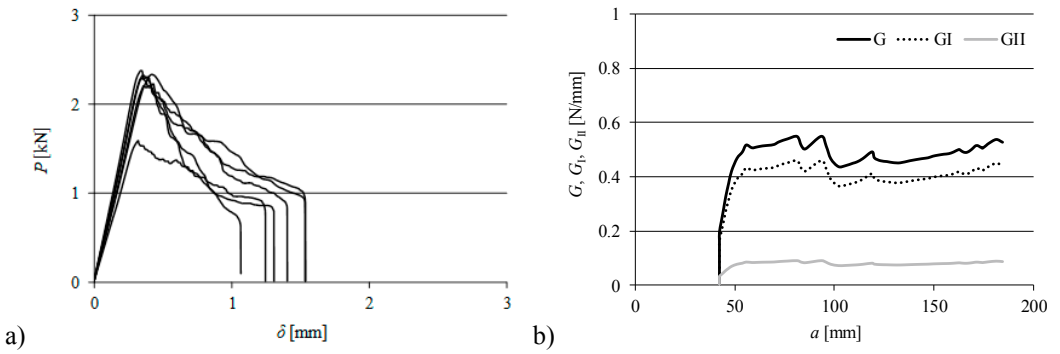

Fig. 3. P-δ curves (a) and R-curves (G, G_I and G_{II}) (b) obtained for the ATDCB specimens.

The overall behaviour of the P-δ curves during the test was also identical between specimens, and this is particularly relevant in the crack growth portion, taking place between P_m and complete failure. The registered P_m and displacements at failure (δ_f) for the ATDCB joints were (the percentile standard deviations are given in parentheses): P_{max}=(2185.5±280.8) N (12.8%) and δ_f=(1.35±0.16) mm (11.8%). The value of G was calculated by equation (3) and the mode partition to estimate G_I and G_{II} was done according to the system of equations (5). An example of R-curves is presented in Fig. 3 (b). All R-curves exhibit constant G_I or G_{II} during crack growth, despite minor oscillations. G_I and G_{II} showed a good concordance between specimens (Table 2). The experimental tests performed with the adhesive Araldite® 2015 allowed to obtain a percentile deviation of the average G_I and G_{II} values under 3%.

Table 2. Individual G_I and G_{II} [N/mm] of the ATDCB tests.

Adhesive	Araldite® 2015	
Specimen	G_I	G_{II}
1	0.431	0.085
2	0.424	0.081
3	0.415	0.083
4	0.431	0.086
5	0.422	0.084
6	-	-
7	0.410	0.079
Average	0.422	0.083
Deviation	0.008	0.002

4.3. Fracture envelope of the adhesive

The best mixed-mode criterion to model adhesive joints with the Araldite® 2015 is assessed by establishing the fracture envelope of the adhesive. A mixed-mode criterion based in expression (6) is selected for the adhesive, such that it can accurately combine the tensile and shear load modes usually found in an adhesive joint. This analysis will assume α=β in expression (6), considering values of 1/2, 1, 3/2 and 2. This analysis is done by comparing the experimental points with these criteria. The idealized fracture envelope for the adhesive Araldite® 2015 and the test points obtained with the ATDCB data are shown in Fig. 4. The curves for this figure were plotted using the pure-mode G_{IC} and G_{IIC} information presented in Section 4.1 in both axes (shear data for the horizontal axis and tensile data to the vertical axis), and considering the four aforementioned α=β values.

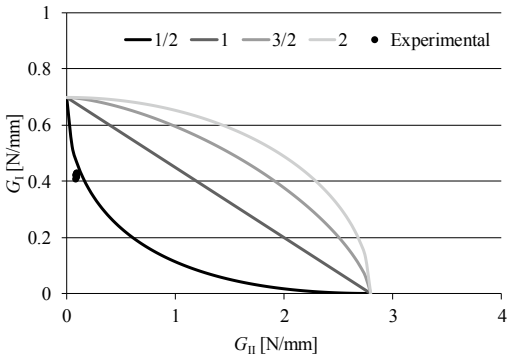

Fig. 4. Experimental fracture envelope.

The experimental G_I/G_{II} data points for the Araldite® 2015 show close results for all specimens. They also enable to easily identify the location of the points characteristic of the Araldite® 2015 in a small zone of the fracture envelope very close of the α=½ criterion's representative curve. This evidence makes α=½ as the most suitable crack growth exponent to be used in the mixed-mode propagation criterion of the Araldite® 2015.

4.4. Modelling the ATDCB tests

The CZM technique is initially applied to compare the P-δ curves between the simulations and experimental tests. With this purpose, numerical models with the individual a_0 values were considered. As previously defined, α=½. Fig. 5 (a) presents a comparison between experimental and numerical P-δ curves for the ATDCB test. Considering all specimens, the average deviations (considering all specimens) in the P_m and maximum load displacement (δP_m) were +7.0% and +87.9%, respectively. Thus, the P_m predictions were accurate. On the other hand, the numerical δ_f highly overshot the experimental tests, which can be explained by experimental defects or voids.

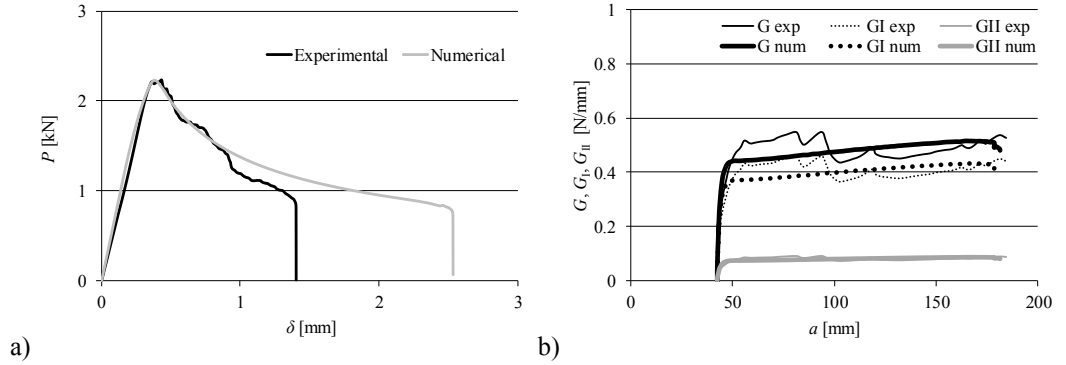

Fig. 5. Example of experimental and numerical P-δ curves (a) and experimental and numerical R curves (b) for the ATDCB test.

Fig. 5 (b) shows the experimental and numerical R-curves after data analysis of the specimen of Fig. 5 (a). This analysis was extended for all specimens, giving an average G, G_I and G_{II} difference in the respective steady-state values of 2.5%. The simulated R-curves captured the experimental behaviour quite accurately. The biggest $G/G_I/G_{II}$ variation was 4.0%, which testifies the capability of the numerical method to calculate G for ductile adhesives.

4.5. Numerical α verification

As the final step of the CZM numerical verification, the numerical fracture envelope of the tested adhesive is compared against the experimental one. Here, the followed methodology consists of introducing the experimentally obtained α in the numerical simulations and attempt to reproduce the experimental α. The gathered data is plotted in Fig. 6 against the ideal fracture envelopes with different α.

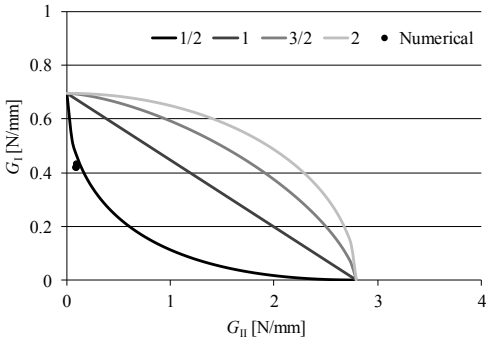

Fig. 6. CZM G_I/G_{II} points in fracture envelopes with different α.

First of all, a smaller scatter of the data points is visible, compared to the experimental points of Fig. 4. Equally to that discussed for the R-curves, this difference takes place because of the numerical models not being affected by

inherently experimental effects, which can artificially induce variations in the measurements. Comparison to Fig. 4 permits to validate the defined crack growth criterion exponent α=1/2, since the numerical data points dwell close to the respective fracture envelope. As a result, the CZM data is considered suitable for the strength prediction of bonded joints under arbitrary geometry and mixed-mode loading.

5. Conclusions

This work aimed at estimating and numerically validating the fracture envelope of a structural adhesive, considering the ATDCB test for this purpose. The first step was the construction of the experimental fracture envelopes, carried out using the data from the P-δ curves. In turn, these and a proper data reduction scheme made possible to obtain the R-curves, which identified G_I and G_{II} for each specimen. Each G_I/G_{II} point was superimposed in the idealized fracture envelopes, making possible to identify the most suitable α for this adhesive. The adhesive was best modelled with α=1/2. This result agrees with published results for the same adhesive [6]. On the other hand, the CZM analysis used this experimental data as input to replicate the test P-δ and R-curves. This resulted in an accurate reproduction of the test results. It can be then concluded that the chosen mixed-mode criteria for the adhesive was successfully validated. This data can now be extrapolated for generic mixed-mode joints for the purpose of strength prediction with this adhesive.

References

[1] L.F. da Silva, A. Öchsner, R.D. Adams. Handbook of adhesion technology: Springer Science & Business Media; 2011.
[2] T. Pardoen, T. Ferracin, C. Landis, F. Delannay, Constraint effects in adhesive joint fracture, Journal of the Mechanics and Physics of Solids, 53 (2005) 1951-83.
[3] D. Xie, A.M. Waas, Discrete cohesive zone model for mixed-mode fracture using finite element analysis, Engineering Fracture Mechanics, 73 (2006) 1783-96.
[4] T. Vallée, J.R. Correia, T. Keller, Probabilistic strength prediction for double lap joints composed of pultruded GFRP profiles–Part II: Strength prediction, Composites Science and Technology, 66 (2006) 1915-30.
[5] S. Park, D.A. Dillard, Development of a simple mixed-mode fracture test and the resulting fracture energy envelope for an adhesive bond, International Journal of Fracture, 148 (2007) 261-71.
[6] L.F.M. da Silva, V.H.C. Esteves, F.J.P. Chaves, Fracture toughness of a structural adhesive under mixed mode loadings, Materialwissenschaft und Werkstofftechnik, 42 (2011) 460-70.
[7] R.D.S.G. Campilho, A.M.G. Pinto, M.D. Banea, L.F.M. da Silva, Optimization study of hybrid spot-welded/bonded single-lap joints, International Journal of Adhesion and Adhesives, 37 (2012) 86-95.
[8] R.D. Campilho, M.D. Banea, J. Neto, L.F. da Silva, Modelling adhesive joints with cohesive zone models: effect of the cohesive law shape of the adhesive layer, International Journal of Adhesion and Adhesives, 44 (2013) 48-56.
[9] R.D.S.G. Campilho, M.D. Banea, A.M.G. Pinto, L.F.M. da Silva, A.M.P. de Jesus, Strength prediction of single- and double-lap joints by standard and extended finite element modelling, International Journal of Adhesion and Adhesives, 31 (2011) 363-72.
[10] A.C.C. Leitão, R.D.S.G. Campilho, D.C. Moura, Shear Characterization of Adhesive Layers by Advanced Optical Techniques, Experimental Mechanics, 56 (2016) 493-506.
[11] C.J. Constante, R.D.S.G. Campilho, D.C. Moura, Tensile fracture characterization of adhesive joints by standard and optical techniques, Engineering Fracture Mechanics, 136 (2015) 292-304.
[12] G.R. Irwin, J.A. Kies, Critical energy release rate analysis of fracture strength, Welding Journal, 33 (1954) 193-8.
[13] ASTM D3433-99 Standard. Standard test method for fracture strength in cleavage of adhesives in bonded metal joints. West Conshohocken, PA: ASTM International; 2012.
[14] H. Luo, Y. Yan, T. Zhang, Z. Liang, Progressive failure and experimental study of adhesively bonded composite single-lap joints subjected to axial tensile loads, Journal of Adhesion Science and Technology, 30 (2016) 894-914.
[15] A.U. Sane, P.M. Padole, C.M. Manjunatha, R.V. Uddanwadiker, P. Jhunjhunwala, Mixed mode cohesive zone modelling and analysis of adhesively bonded composite T-joint under pull-out load, Journal of the Brazilian Society of Mechanical Sciences and Engineering, 40 (2018) 167.
[16] R. Dimitri, M. Trullo, L. De Lorenzis, G. Zavarise, Coupled cohesive zone models for mixed-mode fracture: A comparative study, Engineering Fracture Mechanics, 148 (2015) 145-79.
[17] R.J.B. Rocha, R.D.S.G. Campilho, Evaluation of different modelling conditions in the cohesive zone analysis of single-lap bonded joints, The Journal of Adhesion, (2017) in press.
[18] M. Shahverdi, A. Vassilopoulos, T. Keller, Modeling effects of asymmetry and fiber bridging on Mode I fracture behaviour of bonded pultruded composite joints, Eng Fract Mech, 99 (2013) 335 - 48.
[19] A. Ameli, M. Papini, J.K. Spelt, Fracture R-curve of a toughened epoxy adhesive as a function of irreversible degradation, Materials Science and Engineering: A, 527 (2010) 5105-14.